Low-temperature specific heat, AC susceptibility and magnetisation of the singlet ground-state compounds $TmIr_2$ and $TmRh_2$

1989 J. Phys.: Condens. Matter 1 8181

(http://iopscience.iop.org/0953-8984/1/43/018)

J. Phys.: Condens. Matter **1** (1989) 8181–8197. Printed in the UK

Low-temperature specific heat, AC susceptibility and magnetisation of the singlet ground-state compounds $TmIr_2$ and $TmRh_2$

A F Deutz†, H B Brom†, W J Huiskamp†, L J de Jongh† and K H J Buschow‡

† Kamerlingh Omnes Laboratorium der Rijksuniversiteit Leiden, Postbus 9506, 2300 RA Leiden, The Netherlands

‡ Philips Research Laboratories, 5600 JA Eindhoven, The Netherlands

Received 21 September 1988, in final form 6 April 1989

Abstract. We present low-temperature specific heat, AC susceptibility, magnetisation and resistivity experiments on the intermetallic Laves phase compounds $TmIr_2$ and $TmRh_2$. The experimental susceptibility data below 1 K, both in zero and non-zero magnetic field, show for $TmIr_2$ a transition to a completely diamagnetic state at 0.25 K, indicating the presence of bulk superconductivity below that temperature. For $TmRh_2$ it is found that this compound has a singlet crystal field ground state. $TmRh_2$ undergoes a transition to a ferromagnetic induced moment ordered state at 0.4 K. Based on an analysis of the specific heat data for the two compounds, several possible sets of crystal field parameters are discussed. It appears to be necessary to include the effect of a distortion from cubic symmetry in the Hamiltonian, which is consistent with available Mössbauer data.

1. Introduction

In our systematic study on cubic Tm intermetallic compounds with a singlet ground state we focused on TmA_2 (Laves phase structure) and on TmB_3 ($AuCu_3$ structure) compounds. In this paper we present low-temperature magnetic properties of $TmIr_2$ and $TmRh_2$. The compounds crystallise in the cubic Laves phase structure.

The results of Mössbauer experiments by Gubbens *et al* on $TmRh_2$ and $TmIr_2$ indicated a quadrupolar splitting at low temperature [1]. For $TmRh_2$ this splitting was found to persist until about 100 K. The spectra could be fitted by assuming a $\Gamma_5^{(1)}$ crystal field ground state and a tetragonal distortion ($x = 0.55$, $W/k = 0.7$ K and $B_0^2/k = -0.66$ K; see equations (7) and (8)). For $TmIr_2$ no crystal field parameters were obtained due to the lack of experimental data. In both compounds the observed quadrupolar splitting was ascribed to static or dynamic distortions.

More recently Willis *et al* reported antiferromagnetic ordering of $TmIr_2$ at 50 mK [2]. A small cusp was observed in a curve of the inverse AC susceptibility versus temperature. The position of the cusp moved to lower temperatures when a magnetic field was applied.

0953-8984/89/438181 + 17 $02.50

In this paper we present low-temperature specific heat and AC susceptibility data, in magnetic fields and in zero field, for $TmIr_2$ and $TmRh_2$. The magnetisation at 4.2 K is also determined and for $TmRh_2$ the resistivity is measured from 5 K to about 300 K. In $TmIr_2$ a transition to a completely diamagnetic state is visible in the AC susceptibility at about 0.25 K. This probably indicates a superconducting transition. We propose five sets of crystal field parameters consistent with our specific heat data. For $TmRh_2$ a magnetic phase transition is observed at 0.4 K. This compound shows an induced moment ordering. From the specific heat data, which cannot be reproduced by the set presented by Gubbens *et al* [1], a number of possible sets of parameters have been obtained.

2. Experimental

The polycrystalline $TmIr_2$ and $TmRh_2$ samples were prepared by arc melting in an atmosphere of purified argon, using starting materials of at least 99.9% purity. The sample were wrapped in Ta foil and sealed in an evacuated quartz tube. Vacuum annealing was performed for 1 week at 1100 °C ($TmIr_2$) and 1000 °C ($TmRh_2$). After annealing the $TmIr_2$ sample was rapidly cooled by quenching in water. Owing to the fact that Tm is above its boiling point at the melting point of Ir, the arc melting technique gives rise to serious losses of Tm, leading to a sample consisting of $TmIr_2$ and large amounts of Ir metal. In order to compensate for the loss of Tm an excess of 20% Tm has been found to lead to an acceptable result, although x-ray diffraction showed that there was still a small amount of Ir metal present as a second phase after arc melting. Based on the x-ray intensities of the diffraction peaks of $TmIr_2$ and Ir the amount of the Ir impurity phase was estimated to be about 5%. No significant changes in the relative proportions of the phases $TmIr_2$ and Ir occurred during the homogenisation treatment. The lattice constant derived from the annealed $TmIr_2$ sample is $a = 0.7474$ nm. The same value was found for $TmIr_2$ by Willis *et al* [2]. In the case of $TmRh_2$ the Tm loss during the arc melting is considerably less serious than in the case of $TmIr_2$. In the former case we found that an excess of about 1% was sufficient to produce a single phase sample. The lattice constant derived from the annealed sample is $a = 0.7393$ nm.

The specific heat was measured using the conventional heat pulse technique. The magnetisation in fields up to 5 T was measured in a vibrating sample magnetometer. The AC susceptibility above 1.2 K was determined via the mutual inductance technique [3]. A primary coil produced an oscillating magnetic field with a frequency of 82.9 Hz and a small amplitude. The AC susceptibility in the temperature region 60 mK–5 K was measured in a different apparatus in which the sample remained in one of the secondary coils, which were part of a mutual inductance bridge. The DC resistivity was determined via the standard four wire technique.

3. Results

The specific heat of $TmIr_2$ is presented in figure 1. A correction is made for the contribution from the lattice phonons and the conduction electrons. For this correction we

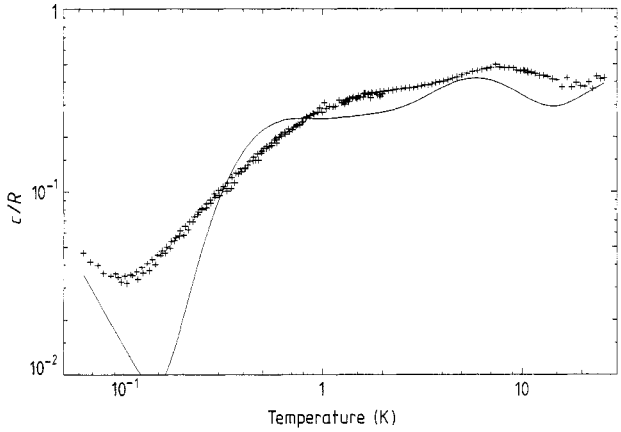

Figure 1. Specific heat, c, versus temperature for $TmIr_2$. The correction for the lattice contribution has already been applied. It is taken from $LaIr_2$ and discussed in the text. The drawn line is calculated using the Hamiltonian parameters of set 1 in table 1. R is the gas constant.

have used the values $\gamma = 6.9\ \text{mJ mol}^{-1}\text{K}^{-2}$ and $\theta_D = 214\ \text{K}$ in the expression for the conduction electron contribution

$$c_E = \gamma T \tag{1}$$

and the lattice contribution

$$c_L = 3nRD\left(\frac{\theta_D}{T}\right) \tag{2}$$

respectively. Here R is the gas constant and $D(\theta_D/T)$ is the (normalised) Debye function. The number of atoms per formula unit is represented by n and amounts to 3 in the case of the Laves phase compounds. The numerical values are the result of a least-squares fit of equations (1) and (2) to the reported specific heat data of the isomorphous non-magnetic compound $LaIr_2$ [4]. The subtracted specific heat ranges from about 1% of the total specific heat at 4 K to a fraction of about 70% at 30 K. At low temperatures, below 100 mK, an increase of the specific heat with decreasing temperature is visible. Apart from this upturn, no anomalies are present in the specific heat curve.

The magnetisation of $TmIr_2$ is measured at 4.2 K in magnetic fields up to 5 T (figure 2). The low field part shows a linear increase of the magnetisation as a function of the magnetic field. Above 0.5 T the slope of the curve decreases, although the magnetisation is clearly not saturated in the maximum field of 5 T.

The inverse AC susceptibility of $TmIr_2$ at temperatures from 1 K up to 150 K is shown in figure 3. It shows a Curie–Weiss behaviour above 4.2 K. The straight line is a least-squares fit of the data above 4.2 K to the equation

$$\frac{1}{\chi} = \frac{T - \theta}{C} \tag{3}$$

and corresponds to values of $-1.8\ \text{K}$ for the Curie–Weiss temperature θ and $7.7 \times 10^{-5}\ \text{K m}^3\text{mol}^{-1}$ for the Curie constant C. The effective moment corresponds to 93% of the value for a free Tm ion. In the inset of figure 3 it is visible that below 4.2 K a small deviation from the straight line occurs.

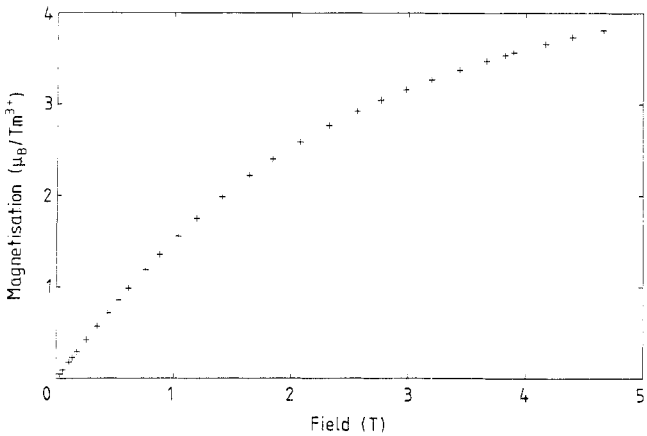

Figure 2. Magnetisation (in μ_B/Tm atom) versus field for $TmIr_2$ at 4.2 K.

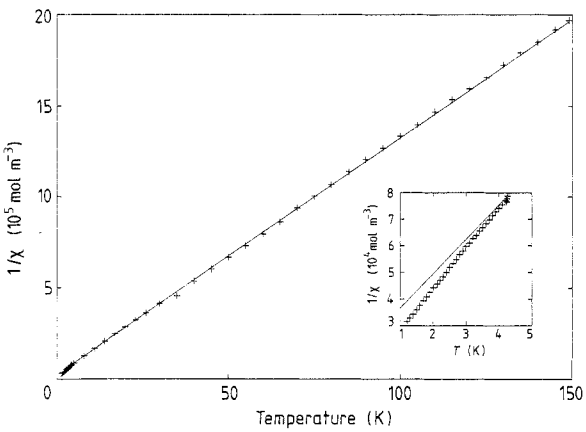

Figure 3. Reciprocal AC susceptibility versus temperature for $TmIr_2$ at temperatures above 1 K. The straight line comes from a least-squares fit of the data above 4.2 K to the Curie–Weiss formula of equation (3). The inset shows a magnification of the left lower corner of the figure, including an extrapolation of the fitted line.

The AC susceptibility of $TmIr_2$ below 1 K shows more interesting features (figure 4). The zero-field data of a small spark-cut slice ($6.5 \times 3.0 \times 0.5$ mm^3) of our polycrystalline $TmIr_2$ sample displays a sharp transition to negative values of the susceptibility at 256 ± 10 mK. In this experiment the direction of the oscillating magnetic field is in the plane of the sample. A second AC susceptibility experiment (figure 5) was performed on another piece of the polycrystalline $TmIr_2$ sample, which now had a pyramid-like shape (the largest dimension being about 4 mm). These measurements have been performed in several different static magnetic fields. The oscillating and static magnetic fields are both directed along the largest side of the sample. In figure 5 the zero-field susceptibility again shows a clear transition at 252 ± 10 mK. The absolute value of the susceptibility at the lowest temperature exceeds the value reached for the flat sample (figure 4). In increasing static magnetic field, the transition becomes less pronounced and shifts to lower temperatures. Finally it disappears for magnetic fields above 36 mT.

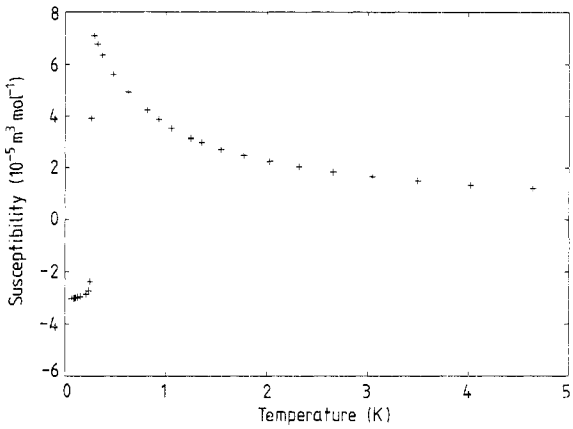

Figure 4. AC susceptibility versus temperature for $TmIr_2$ at low temperatures. These data refer to measurements on the flat sample discussed in the text.

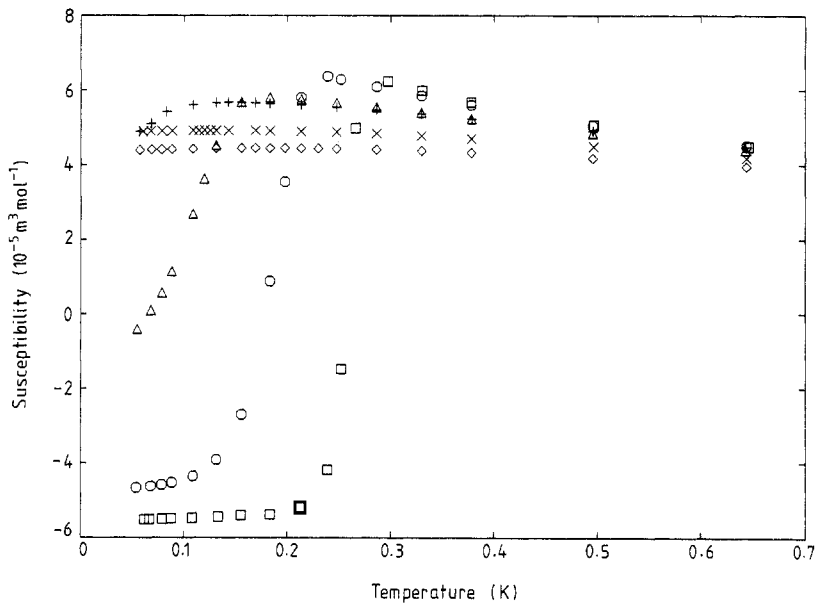

Figure 5. AC susceptibility of $TmIr_2$ versus temperature in several static magnetic fields ranging from 0 mT to 59 mT. These data are measured on the pyramid (shaped) sample which is discussed in the text. The symbols correspond to the magnetic field used: □, 0 mT; ○, 12 mT; △, 24 mT; +, 36 mT; ×, 48 mT; ◇, 59 mT.

The AC susceptibility of $TmIr_2$ at a fixed temperature of 72 mK as a function of the static magnetic field is presented in figure 6. The experiments were done on the flat sample.

The AC susceptibility of $TmRh_2$ is shown in figure 7. In the zero-field data a maximum is visible at a temperature of 0.40 ± 0.02 K. In a small static magnetic field of 0.12 T the AC susceptibility decreases considerably, while the position of the maximum is shifted to a temperature of 1.0 ± 0.1 K. At temperatures above 2 K the data in 0.12 T coincide

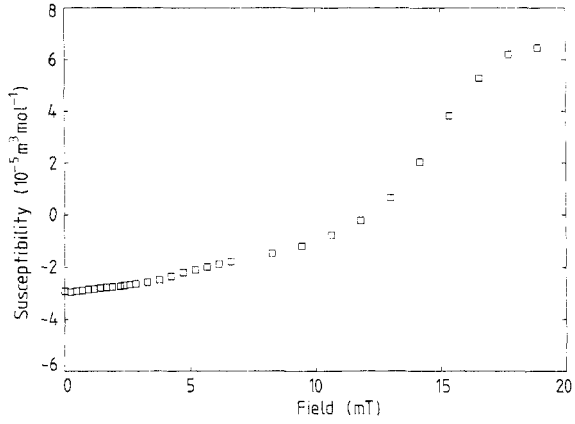

Figure 6. AC susceptibility versus applied magnetic field for $TmIr_2$ at a temperature of 72 mK. The experiment is done on the flat sample. The vertical axis is scaled by comparison with figure 5.

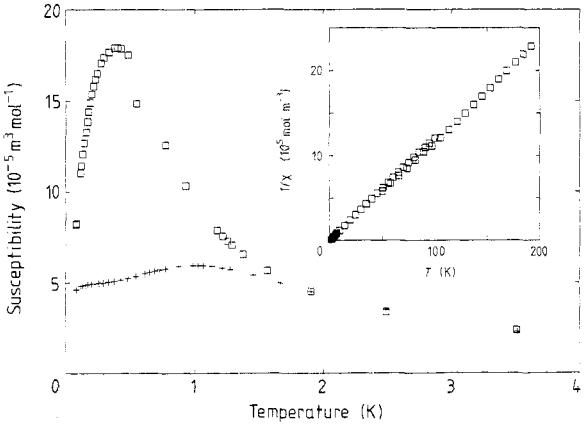

Figure 7. AC susceptibility versus temperature for $TmRh_2$. The data obtained in a static magnetic field of 0 T are represented by □ while + correspond to the data in a field of 0.12 T. The inset shows the inverse AC susceptibility versus temperature obtained from experiments in several temperature ranges.

with the zero-field AC susceptibility, which shows a Curie–Weiss behaviour until 200 K. From a least-squares fit of the Curie–Weiss law (equation (3)) to the experimental data in the temperature region 4–200 K values of $\theta = -0.04$ K and $C = 8.4 \times 10^{-5}$ K m^3 mol^{-1} (corresponding to 97% of the effective moment for a free Tm^{3+} ion) have been obtained for the Curie–Weiss temperature and Curie constant respectively.

The magnetisation of $TmRh_2$ is presented in figure 8. The maximum value of 7 μ_B/Tm^{3+} is not yet reached in the highest field of 5 T.

Figure 9 shows the specific heat of $TmRh_2$ in the temperature range 72 mK–29 K. The reported specific heat of $LaRh_2$ is subtracted from the measured specific heat with the purpose of accounting for the contributions from the lattice phonons and conduction electrons. For this correction the values of $\gamma = 3.3$ mJ mol^{-1}K^{-2} and $\theta = 232$ K [4] have

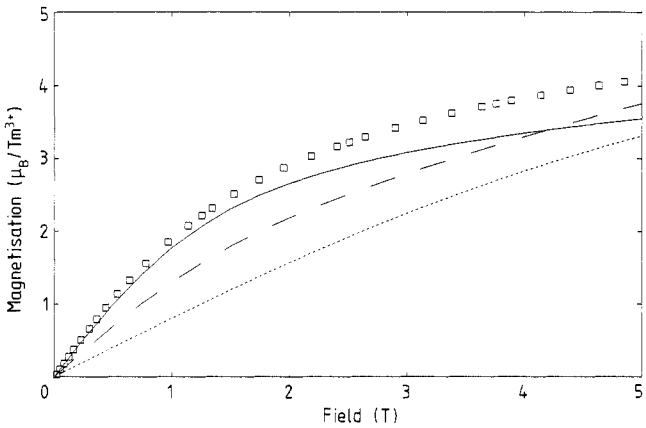

Figure 8. Magnetisation (in μ_B/Tm^{3+}) versus field for $TmRh_2$ at 4.2 K. The curves are calculated using the parameters of set 1 (full curve), set 3 (broken curve) and set 4 (dotted curve) from table 2.

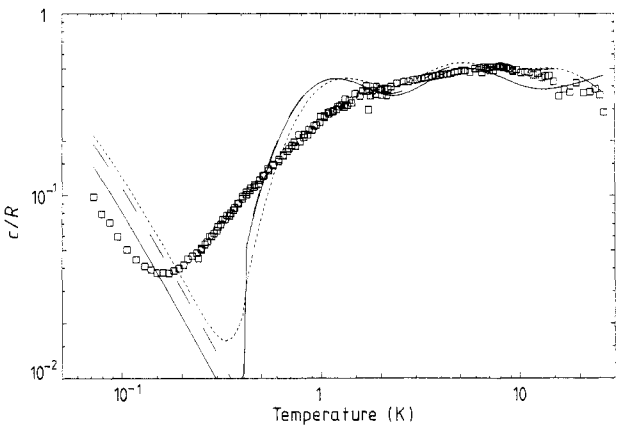

Figure 9. Specific heat, c, versus temperature for $TmRh_2$. The data have already been corrected for the lattice phonons and conduction electron contributions by using the γ and θ_D values for $LaRh_2$ as discussed in the text. The curves are calculated using the parameter set in table 2: set 1 (full curve), set 3 (broken curve) and set 4 (dotted curve). The gas constant is denoted by R.

been substituted in equations (1) and (2) respectively. The non-magnetic contribution to the total specific heat of $TmRh_2$ ranges from about 2% at 5 K to about 80% at 29 K.

The measured resistivity data for $TmRh_2$ are collected in figure 10. The derivative of the resistivity with respect to the temperature shows a change in slope at around 60 K. The structure seen at about 75 K may not be a real effect. The small bumps in $\partial\rho/\partial T$ at the highest temperatures are ascribed to small experimental errors (not visible in the inset of figure 10) in the measured resistivity at these temperatures.

4. Discussion of the $TmIr_2$ data

The observed transition to negative values of the zero-field AC susceptibility can be explained by assuming a transition to a state of perfect diamagnetic shielding below

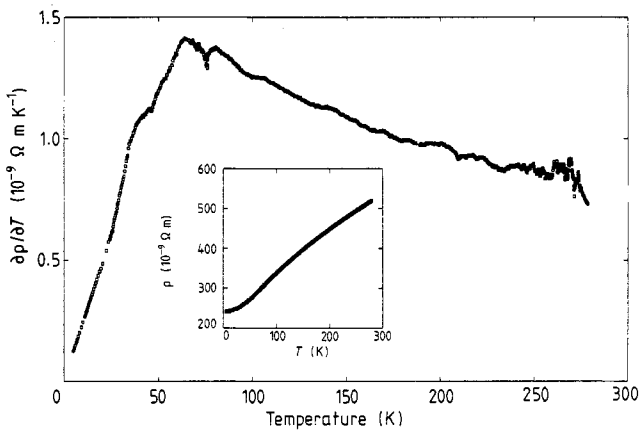

Figure 10. Temperature derivative $\partial\rho/\partial T$ of the resistivity of $TmRh_2$. The measured resistivity ρ, from which the derivative is obtained, versus the temperature T is shown in the inset.

250 mK. There are no resistivity data available in this temperature range. However, the explanation in terms of (apparently) perfect diamagnetism is supported by a calculation of the expected diamagnetic susceptibility from the estimated demagnetising factor of the samples. For the flat sample of figure 4 the demagnetising factor N is very close to zero, because of the direction of the oscillating field parallel to the planer surface of the sample. An estimate for the density ρ can be based on the lattice constant of $TmIr_2$ at room temperature:

$$\rho \approx \frac{8M}{N_A a^3} = 18 \times 10^3 \text{ kg m}^{-3}. \tag{4}$$

In this expression N_A and M represent the Avogadro number and the molecular weight of $TmIr_2$, respectively. The cubic unit cell contains 8 molecules and has a lattice constant a of 0.7474 nm. The susceptibility of a diamagnetic sample can then be expressed in terms of the demagnetising factor:

$$\chi_{\text{dia}} = \frac{-f}{1 - N\rho}\frac{M}{} \tag{5}$$

where f denotes the diamagnetic fraction of the sample. The susceptibility is then expressed in the units $m^3\,mol^{-1}$. Inserting the numerical values for the flat sample in equation (5) leads to $f = 1.0$. If the same diamagnetic 'fraction' f is adopted for the pyramid-like shaped sample of the data in figure 5, a demagnetising factor $N = 0.45$ follows from equation (5), which seems to be a reasonable value. It can be concluded from the above argument that a practically complete diamagnetic shielding is present in both samples.

It has recently been pointed out by Hein [5, 6] that the observation of a diamagnetic AC susceptibility is not sufficient for discerning between bulk and non-bulk superconductivity. When an AC susceptibility technique is used, bulk superconductivity can be shown by the additional experiment of AC susceptibility as a function of the external magnetic field at a fixed temperature. If the so called differential paramagnetic effect (DPE) [5] is found, then it may be concluded that a Meissner effect is present. The data

presented in figure 6 do not unambiguously show a DPE. Unfortunately AC susceptibility data at that temperature are not available for magnetic fields higher than those used in figure 6. At the highest field (20 mT), the susceptibility only seems to reach a stable value. It is therefore not possible yet to decide whether $TmIr_2$ is indeed a bulk superconductor below 0.25 K, although this seems to be quite probable.

The field dependence of the AC susceptibility of the flat sample at the low temperatures of 72 mK (figure 6) does suggest a classification of $TmIr_2$ as a type II superconductor. The lower critical field H_{C1} is of the order of a few mT, while the H_{C2} value can be estimated to be of the order of 20 mT. For the pyramidal shaped sample, the lower critical field is below 12 mT, while the higher critical field is of the order of 48 mT. At temperatures above 1.2 K, the AC susceptibility in the magnetic fields up to 59 mT is indistinguishable from the zero-field data. It should be noted that the larger value of the paramagnetic susceptibility of the flat sample (e.g. at 20 mT in figure 6) as compared to the values obtained for the pyramid shaped sample (figure 5) can be explained by the difference in the demagnetising factors.

Our AC susceptibility data at low temperatures do not confirm the single crystal data reported by Willis *et al* [2]. The increase in the slope of their $1/\chi$ versus T curve at 300 mK is not visible in the zero-field curve of figure 5. Furthermore, Willis *et al* report a cusp in their curve at 50 mK, which was ascribed in an anti-ferromagnetic ordering. It is not mentioned whether the AC susceptibility was measured in a non-zero static magnetic field, but in any case a discrepancy with our data remains.

The deviation from Curie–Weiss behaviour in the AC susceptibility below 4 K can be ascribed to crystal field effects, the temperature probably being of the same order of magnitude as the energy splitting between the lowest lying levels.

The magnetisation data of $TmIr_2$ shows a behaviour which is comparable to the magnetisation of the isostructural compound $TmNi_2$ [7], where the magnetisation gradually increases for magnetic fields from 5 T to 30 T. So it can be expected that the maximum value of 7 μ_B for the Tm^{3+} magnetic moment in $TmIr_2$ is only reached in much larger fields than the applied maximum of 5 T. The susceptibility which can be calculated from the slope of the magnetisation between 0 T and 0.5 T, assuming a linear behaviour, agrees with the measured zero-field AC susceptibility at 4.2 K within 12%.

The analysis of the specific heat data of $TmIr_2$ is mainly based on an entropy calculation, where the entropy is derived from

$$S(T_1, T_2) = R \ln g_0 + \int_{T_1}^{T_2} \mathrm{d}T \frac{c(T)}{T}. \tag{6}$$

In this expression, the entropy is calculated between the temperatures T_1 and T_2, where in the ideal case T_1 equals 0 K. In practice T_1 is the lowest temperature at which experimental specific heat data is available. Below T_1, the integrand should be small enough to be negligible. The number of states in the system having energies below T_1 is represented by g_0; if T_1 is very low then g_0 is the ground state degeneracy. R is the gas constant. The total number of states for the electronic and nuclear Tm^{3+} system is 26 (Tm^{3+}: $J = 6$ and $I = 1/2$), corresponding to an entropy of $R \ln 26$.

It is clear from the specific heat of $TmIr_2$ in figure 1, that at the lowest temperature the value of the integrand $c(T)/T$ in equation (6) cannot be neglected. It is therefore necessary to subtract a low temperature specific heat Schottky anomaly from the experimental data. The upturn in the specific heat curve at the lowest temperatures is then treated as the high temperature tail of this Schottky anomaly. A Schottky anomaly

corresponding to an energy splitting of the lowest lying levels of 28 ± 2 mK accounts reasonably for the observed upturn in the specific heat. After subtracting this Schottky anomaly from the experimental data, a value of $R \ln 5$ has been obtained for the contribution from the second right hand term in equation (6) to the experimental entropy S (0 K, 30 K). Taking into consideration the total available entropy of $R \ln 26$ and the fact that an additional entropy contribution is to be expected from temperatures above 30 K, we may conclude that the maximum value for g_0 equals 4.

As a first step in obtaining the crystal field parameters for $TmIr_2$ from an analysis of the specific heat, we want to discuss the origin of the upturn in the specific heat at the lowest temperatures.

The cubic crystal field only ground state of $TmIr_2$ is either a $\Gamma_5^{(1)}$ triplet or a Γ_1 singlet [1]. Both situations are possible for the range of observed Lea, Leask and Wolf (LLW) [8] parameters x and W for other TmX_2 compounds. The hyperfine interaction can be the cause of the low temperature level splitting if either the electron spins are magnetically ordered or the crystal field state involved has an intrinsic magnetic moment. A further complicating factor is a possible distortion from the cubic structure which can be inferred from e.g. the Mössbauer experiments on $TmIr_2$ [1]. A distortion leads to a splitting of the crystal field levels.

The case of a magnetic ordering in $TmIr_2$ is very well possible from the viewpoint of the entropy discussion. The removal of the nuclear degeneracy in the situation of a singlet CEF ground state due to the internal field leads to the small observed energy splitting. The corresponding Schottky anomaly which has been subtracted into the entropy calculation now accounts for two low-lying levels ($g_0 = 2$). However, this situation would exclude the possibility of bulk superconductivity in $TmIr_2$ (see the foregoing discussion on the susceptibility data).

In the case of no magnetic ordering, the possible situations have to be considered in more detail. From the entropy calculation it follows that the CEF ground state cannot be a (degenerate) Γ_5 triplet. As a result of the hyperfine interaction this situation (considered as an $S = 1$, $I = 1/2$ system) leads to a splitting in a four-fold and two-fold degenerate level. This corresponds to a value of g_0 which is too high ($g_0 = 6$). The only other possibility involving the hyperfine interaction is then a (magnetic) doublet CEF ground state originating from a splitting of the Γ_5 triplet. This splitting then has to be caused by a tetragonal (or trigonal) distortion of the cubic symmetry, leading to a non-degenerate and a two-fold degenerate crystal field level. If the hyperfine interaction is taken into account (considering the lowest states as an $S = 1/2$, $I = 1/2$ system), one observes a splitting in two two-fold degenerate levels ($g_0 = 4$). Although preliminary calculations indicated that the energy splitting in this situation is of the order of 100 mK, we did not exclude this possibility from the fits described below. A final possibility in the case of the absence of a magnetic ordering is a crystal field singlet ground state: the Γ_1 crystal field state or a state originating from the Γ_5 triplet combined with a distortion from cubic symmetry. In this situation the low temperature level splitting is caused by the crystal field and not by the hyperfine interaction. The two lowest, closely lying, levels are the Γ_1 state and one state from the Γ_5 triplet. The nuclear degeneracy is not removed ($g_0 = 4$).

The basic difference between the situations which remain possible from the point of view of the above discussed entropy argument, is the presence of a magnetic transition in $TmIr_2$. Such a transition should occur in the temperature range between 100 mK (where the assumed hyperfine contribution to the specific heat becomes visible) and

250 mK (the superconducting transition temperature). In the case of no magnetic ordering, the energy splitting between the two lowest lying crystal field levels should be about 28 mK.

Next we shall discuss some possible sets of Hamiltonian parameters leading to such a CEF energy splitting. The usual equation for the crystal field Hamiltonian is used [8]:

$$\mathcal{H}_{\mathrm{CEF}} = W\left[\frac{x}{F_4}(O_4^0 + 5O_4^4) + \frac{1-|x|}{F_6}(O_6^0 - 21O_6^4)\right] \tag{7}$$

where x and W are the so called LLW parameters and O_l^m denotes a Steven's operator equivalent, using the definitions of Hutchings [9]. F_4 and F_6 are numerical factors, common to all matrix elements of O_4 and O_6. A possible distortion from cubic symmetry is taken into account by second order operator equivalents:

$$\mathcal{H}_{\mathrm{D}} = B_2^0 O_2^0 + B_2^2 O_2^2 \tag{8}$$

where B_2^0 and B_2^2 are adjustable parameters representing the strength of the distortion. The total Hamiltonian $\mathcal{H}$ is completed with a hyperfine term $\mathcal{H}_{\mathrm{HF}}$:

$$\mathcal{H} = \mathcal{H}_{\mathrm{CEF}} + \mathcal{H}_{\mathrm{D}} + \mathcal{H}_{\mathrm{HF}} \tag{9}$$

where

$$\mathcal{H}_{\mathrm{HF}} = A\boldsymbol{I}\cdot\boldsymbol{J} \tag{10}$$

and A is the hyperfine constant ($A/k = 18.7$ mK [10]). Inspection of the shape of the experimental specific heat curve between 0.1 K and 1 K (see figure 1) shows that it differs considerably from the exponential shape of the low-temperature side of a Schottky anomaly. In that temperature range, the experimental specific heat resembles a power law behaviour. This can be explained by the presence of spin-wave like excitations in the system, which also can occur in the paramagnetic regime. These contributions to the specific heat are not taken into account in the Hamiltonian of equation (9). For this reason we have followed a two-step approach.

First we have selected those x, W, B_2^0, B_2^0 parameters that not only reproduce the experimental specific heat curve above 1 K, but also lead to a calculated specific heat curve which is as close as possible to the experimental values below 1 K. In order to find these parameters an attempt was made to fit the calculated specific heat to the experimental specific heat over the whole temperature range in figure 1. The specific heat is calculated using the Hamiltonian of equation (9) and four adjustable parameters: x, W, B_2^0 and B_2^2. In order to find an initial estimate of the parameters, a part of the 4-dimensional (x, W, B_2^0, B_2^0) parameter space was scanned by varying each parameter independently in small steps. For each set, the calculated specific heat was compared with the experimental data. In the scans, the range of x was limited to the region $0.3 < x < 0.8$. The x value of $TmIr_2$ is expected to be in this range. It is usually observed that the x and W crystal field parameters for isomorphous compounds are comparable and the obtained x value for e.g. $TmAl_2$ is 0.46 [11]. Furthermore, scaling of the crystal field parameters of the Pr Laves phase compounds [12] also leads to an x-value in this range. For the same reasons, the region of the W parameter was restricted to $0\ \mathrm{K} < W/k < 2.0\ \mathrm{K}$. The region of the distortion parameters, B_2^0 and B_2^2, was chosen to be $|B_2^0/k| < 2.0$ K and $0 < B_2^2/k < 2.0$ K. The scans of the (x, W, B_2^0, B_2^2) parameters space did not lead to an acceptable set of parameters, in spite of the very small step (0.001) used in some promising regions. Based on a total of over 100 000 comparisons

Table 1. Possible sets of crystal field parameters for $TmIr_2$. These sets are found from the fitting procedure of the specific heat as discussed in the text. The value $A/k = 18.7$ mK has been used for the hyperfine constant.

Set	x	W/k (K)	B_2^0/k (K)	B_2^2/k (K)
1	0.654	0.642	−0.230	0.357
2	0.644	0.663	−0.220	0.295
3	0.657	0.563	0.273	0.124
4	0.651	0.616	0.270	0.156
5	0.651	0.513	−0.169	0.298

we conclude that there exists no set of parameters, restricted to the regions described above, which reproduces the experimental specific heat in the whole temperature range.

In the next step we have allowed large deviations between the calculated and experimental specific heat in the temperature region of 0.1–1 K. In this approach we kept the low temperature Schottky anomaly (splitting 28 mK) as an important feature of the specific heat curve. To this end we have selected one of the parameter sets which were found to describe the experimental specific heat above 1.0 K and varied the energies of the lowest lying levels in such a way that the splitting between the ground state and the first excited state was 28 mK. This provided a calculated curve, denoted by E', of a similar shape as the drawn line in figure 1. This calculated curve E' was now used to replace the experimental data in the scans and a second attempt was made to find a set of parameters (x, W, B_2^0, B_2^2). If a possible set was found in the scans, the values of the parameters were refined in a least-squares fitting procedure. In this fit, the calculated specific heat was fitted to the previously calculated curve E'. In this way five possible sets of parameters (x, W, B_2^0, B_2^2) were found. The values of the parameters are listed in table 1.

The calculated specific heat curves for the sets of parameters are almost indistinguishable on the scale of figure 1, therefore we have only shown the result for set 1. The overall crystal field splitting is about 100 K for all sets in table 1.

The calculated curve agrees with curve E' (discussed above) in the temperature range below 1 K. At higher temperatures some deviations occur, but the experimental curve is still followed. It can also be expected that other parameter sets can lead to an agreement between calculation and experiment similar to that in figure 1. The suggested accuracy of the parameters in table 1 is also misleading. It only serves to obtain the required splitting of the lowest levels (see below) and has no use in the high temperature region. It is not possible to select one of the five sets in table 1 from a comparison between the calculated and experimental magnetisation. For all five sets the calculated magnetisation is about equal and exceeds the experimental values between 0 and 5 T.

The crystal field ground state for the cubic part of the Hamiltonian ($B_0^2 = B_2^2 = 0$) is for all five sets the Γ_1 singlet. The next higher energy levels are a $\Gamma_5^{(1)}$ and a Γ_4 triplet. The non-zero value of the distortion parameters B_2^0 and B_2^2 causes a splitting of each triplet into three singlets. As a result, the energy splitting between the Γ_1 singlet and one of the states originating from the triplets decreases from a few K (for $B_2^0 = B_2^2 = 0$) to 28 mK. A small change in one of the parameters has a large effect on the final splitting of 28 mK. The values are comparable to those in other Tm intermetallic compounds such as $TmRh_2$ and $TmIn_3$ [13].

The origin of the distortion cannot be revealed by our specific heat experiments. The distortion can be static, like in the case of $TmNi_2$ [14], or dynamic [1]. In the latter situation it seems possible that the specific heat reflects the average value corresponding to two possible lattice structures. The possibility of the presence of a static distortion in the temperature range of our specific heat data should be further investigated by means of e.g. X-ray diffraction at low temperatures. It is also possible that quadrupolar pair interactions are present in $TmIr_2$, like in the case of $ErNi_2$ [15]. Equation 8 serves to take all these possibilities into account.

In the foregoing evaluation of the Hamiltonian parameters we have assumed that no magnetic ordering is present in $TmIr_2$ (see the discussion on the entropy). The other possibility, a magnetically ordered state instead of a paramagnetic state below 250 mK, requires further investigations. A complication is the diamagnetic shielding state of $TmIr_2$ at these low temperatures. A possible, but experimentally complicated tool for the detection of the magnetic transition could be ^{169}Tm Mössbauer spectroscopy at temperatures of the order of 50 mK.

Finally we would like to mention that the absence of a peak in the specific heat of $TmIr_2$ at the proposed superconducting transition temperature of 250 mK is easily understood when the value of the electronic specific heat at that temperature is calculated. The discontinuity in the specific heat can then be estimated as a fraction of only 0.3% of the observed (magnetic) specific heat.

5. Discussion of the $TmRh_2$ data

The AC susceptibility of $TmRh_2$ (figure 7) indicates a magnetic transition at a temperature of about 0.4 K. The decrease in the zero-field AC susceptibility can be ascribed to an anisotropy effect in our polycrystalline sample. An additional effect which may decrease the susceptibility in the ordered region is the influence of the measuring frequency. We did not investigate this any further. The value of the maximum in the zero AC susceptibility corresponds to a demagnetising factor $N \approx 0.17$. This is a reasonable value for our irregularly shaped sample. The large decrease in the value of the AC susceptibility upon applying a static magnetic field agrees with an explanation of the susceptibility of $TmRh_2$ in terms of a ferromagnetic ordering at about 0.4 K. This is also supported by the observed shift of the position of the maximum in the susceptibility to higher temperatures when a magnetic field is applied. The magnetic field strength (0.12 T) exceeded the estimated value of the demagnetising field (0.1 T at the lowest temperatures).

The specific heat data of $TmRh_2$ (figure 9) do not show any anomaly around 0.4 K, the temperature of the magnetic transition. This can be explained in terms of an induced moment magnetic ordering (see e.g. [16, 17, 18]). This situation arises when the crystal field ground state is a singlet state. The ratio between the exchange interaction and the energy splitting of the lowest lying states is a characteristic parameter for this type of systems. Below a certain value for this ratio no magnetic ordering occurs. It is very well possible that this is the situation in the compound $TmIr_2$ (see section 4). If the ratio is close to the threshold, the hyperfine interaction between the electronic and nuclear moments can also play an important role in the ordering. This seems to be the case in $TmRh_2$, where the ordering is situated in the temperature region between the Schottky anomalies due to the depopulation of the electronic system and of the nuclear system, respectively. In such a situation the ordering, if any, occurs at a temperature which is

low in comparison to the temperature (energy) of the first excited crystal field state. This means that the change in entropy at the transition is very low because of the almost 100% population of the ground state at that temperature. Consequently there is no omaly visible in the specific heat. A similar situation was shown to occur in the isomorphous compound $TmNi_2$ [7], where the ferromagnetic ordering occurred at 1.1 K.

The upturn in the specific heat of $TmRh_2$ at the lowest temperatures is explained in terms of a magnetically ordered system. The increase in the specific heat corresponds to the two-level Schottky anomaly which arises from the removal of the nuclear degeneracy of the singlet ground state. This degeneracy is removed due to the internal magnetic field from the electronic moment which acts on the nuclear $I = 1/2$ system via the hyperfine interaction. The hyperfine Hamiltonian of equation (10) can now be represented as

$$\mathcal{H}_{\mathrm{HF},2} = AI_z\langle J_z\rangle \tag{11}$$

where $\langle J_z\rangle$ denotes the thermal average of the magnetic moment operator. The ordering is assumed to be in the z direction. From a least-squares fit of a two-level Schottky anomaly to the experimental specific heat data at the lowest temperatures, it is found that the energy splitting between the nuclear sublevels of $TmRh_2$ is about 48 mK. This corresponds to $\langle J_z\rangle = 2.55$, which should be compared to the maximum possible value of 6.

In order to be able to calculate the specific heat below the transition temperature, we introduce the molecular field Hamiltonian:

$$\mathcal{H}_{\mathrm{MF}} = -g_J\mu_{\mathrm{B}}B_zJ_z + (\lambda/2)\,(g_J\mu_{\mathrm{B}}\langle j_z\rangle)^2 \tag{12}$$

where

$$B_z = g_J\mu_{\mathrm{B}}\lambda\langle j_z\rangle \tag{13}$$

is the molecular field. It depends on the value of the molecular field constant λ and on the self-consistently calculated thermal average of the magnetic moment. The g-factor of Tm^{3+} is represented by g_J, while μ_{B} denotes the Bohr magneton.

We have tried to obtain a set of crystal field parameters from the specific heat of $TmRh_2$. The results of this attempt will now be presented. For the total Hamiltonian we have used

$$\mathcal{H} = \mathcal{H}_{\mathrm{CEF}} + \mathcal{H}_{\mathrm{D}} + \mathcal{H}_{\mathrm{HF},2} + \mathcal{H}_{\mathrm{MF}} \tag{14}$$

where the right hand terms have been defined in equation (7), (8), (11) and (12) respectively. The fitting was initially done in a 4-dimensional parameter space (x, W, B_2^0, B_2^2), keeping λ fixed at zero. The Schottky anomaly due to the hyperfine interaction was first subtracted from the experimental data. The resulting data over the whole temperature range from 100 mK to 30 K were used in the scanning and fitting procedure (described in section 4). This turned out to be necessary because of the large deviations which occurred when the specific heat was calculated at the lowest temperatures using parameters obtained from fits in the temperature region above 0.4 K. As a result of the fitting procedure four sets of parameters have been obtained.

Table 2. Possible sets of crystal field parameters for $TmRh_2$, obtained from fitting the specific heat as discussed in the text. The energy of the first excited level (E_1, $\lambda = 0$) and the value of the molecular field constant λ are also listed.

Set	x	W/k (K)	B_2^0/k (K)	B_2^2/k (K)	E_1/k (K)	λ (10^{23} T A^{-1} m^{-2})
1	0.677	1.31	1.27	0.682	2.84	4.53649
2	0.682	1.34	1.35	0.684	2.84	4.74295
3	0.570	2.60	0.236	0.400	2.81	1.88765
4	0.604	3.28	−0.184	0.551	2.81	1.15168

The values for these sets are listed in table 2. The calculated specific heat curves corresponding to the sets 1, 3 and 4 are shown in figure 9. The curves for set 1 and 2 coincide on the scale of figure 9. The parameters for the sets 1 and 2 also show little differences. They correspond to a different (sub)minimum in the fitting procedure, but the size of the difference may be taken as an indication of the accuracy in the parameters. The energy value of the first excited crystal field level (E_1) is for all sets about the same at 2.8 K. This is relatively high compared to the transition temperature 0.4 K of $TmRh_2$, as can be expected in the case of an induced moment ordering which does not show an anomaly in the specific heat. It should be noted that each set has a singlet ground state, where the ground state for set 3 originates from a $\Gamma_5^{(1)}$ triplet. The other sets have a Γ_1 singlet ground state.

All sets in table 2 have non-zero values for the distortion parameters B_2^0 and B_2^2. So it seems necessary to assume a distortion from cubic symmetry in the temperature range below 30 K (the upper limit of our specific heat experiment). The calculated thermal average $\langle O_2^0 \rangle$ at 4.2 K amounts to about −26 for the sets 1 and 2 in table 2. This agrees within 20% with the value obtained from the quadrupolar splitting in the Mössbauer data by Gubbens *et al* [1]. The correspondence for the sets 3 and 4 is less favourable.

Despite the inclusion of distortion parameters, some deviations between the experiment and calculated specific heat (figure 9) data still exist. At the lowest temperatures this can be ascribed to the occurrence of spin-wave like excitations, while the deviations at the higher temperatures indicate that possibly Tm positions with different site symmetry are present in the distorted state. This effect is observed in $TmNi_2$ at 4.2 K and at room temperature [14].

The molecular field constant λ has been found by adjusting its value until the transition occurred at 0.40 ± 0.02 K.

A further selection between the parameter sets in table 2 can be obtained from a comparison between the calculated and experimental data for the magnetisation (see figure 8) and susceptibility. The magnetisation as well as the susceptibility have been calculated by adding the values obtained for the magnetic field in the x-, y- and z-direction with equal weight. This is performed in order to account for the polycrystalline character of our $TmRh_2$ sample. On the basis of a magnetisation comparison (see figure 8), the parameters of set 4 (see table 2) are less favourable for the description of the $TmRh_2$ data. This set 4 also shows the largest deviations in the susceptibility comparison. The agreement between calculated and experimental magnetisation for set 3 is also less than for the sets 1 and 2. The susceptibility however does not show much difference for the sets 1, 2 and 3.

Finally, a rough interpretation of the resistivity data allows for the selection of the sets 1 and 2 in favour of set 3. From the relation between the dynamic susceptibility and the resistivity [19] it follows that the temperature derivative of the resistivity is related to the specific heat. The temperature derivative of the resistivity reflects the energies of the crystal field states. Following this argument, energy levels for $TmRh_2$ should be present at about 80 K. The sets 1, 2 and 3 all have energy levels around 50 K. The next higher level for set 3 is already at around 280 K, while set 1 and 2 contain two levels at about 80 K.

6. Conclusion

The intermetallic compound $TmIr_2$ shows perfect diamagnetic shielding at temperatures below about 0.25 K, which may indicate the presence of bulk superconductivity below that temperature. The specific heat at the lowest temperatures increases with decreasing temperature. This is interpreted as the onset of a two-level Schottky anomaly corresponding to a very small splitting (only 28 mK) of the lowest crystal field energy levels. The small splitting seems to be the resulting splitting between the Γ_1 ground state and the lowest state of the next higher triplet. This triplet is split due to distortions or magneto-elastic effects, the lowest state coincidentally being almost degenerate with the singlet ground state. Another possibility which cannot be completely ruled out is a transition to a magnetically ordered state between about 100 mK and 250 mK. This latter possibility and the more precise nature of the distortions require further investigations.

Our experimental data for $TmRh_2$ show that this compound undergoes a transition to a ferromagnetic state at 0.4 K. The ordering has been classified as an induced moment ordering, involving an energy separation between the two lowest lying singlet crystal field states which is large in comparison to the transition temperature. From an analysis of the specific heat data four possible sets of crystal field parameters have been obtained. A further selection to set 1 and 2 in table 2 has been reached by taking the magnetisation and susceptibility into consideration. For these sets the calculated quadrupolar splitting agrees reasonably with the value obtained from the Mössbauer data [1]. The existence of other parameter sets, for $TmRh_2$ as well as for $TmIr_2$, cannot be excluded. Inelastic neutron scattering experiments might provide additional information.

Acknowledgments

We would like to acknowledge L Koene and G M J van Soest for their assistance during the experiments.

This work is part of the research programme of the Stichting voor Fundamenteel Onderzoek der Materie (Foundation for Fundamental Research on Matter) and was made possible by financial support from the Nederlandse Organisatie voor Zuiver Wetenschappelijk Onderzoek (Netherlands Organisation for the Advancement of Pure Research).

References

[1] Gubbens P C M, van der Kraan A M and Buschow K H J 1984 *J. Phys. F: Met. Phys.* **14** 2195–201

[2] Willis J O, Smith J L and Fisk Z 1985 *J. Magn. Magn. Mater.* **47–48** 581–2
[3] Deutz A F, Hulstman R and Kranenburg F J 1989 *Rev. Sci. Instrum* **60** 113
[4] Greidanus F J A M, Nieuwenhuys G J, de Jongh L J, Huiskamp W J, Capel H W and Buschow K H J 1983 *Physica* B **119** 228–42
[5] Hein R A and Falge R L Jr 1961 *Phys. Rev.* **123** 407–15
[6] Hein R A 1986 *Phys. Rev.* B **33** 7539–49
[7] Deutz A F, Brom H B, Deelen H, de Jongh L J, Huiskamp W J and Buschow K H J 1986 *Solid State Commun.* **60** 917–21
[8] Lea K R, Leask M J M and Wolf W P 1962 *J. Phys. Chem. Solids* **23** 1381–405
[9] Hutchings M T 1964 In *Solid State Phys.* ed. F Seitz and D Turnbull (New York: Academic) pp 227–73
[10] Bleaney B 1972 In *Magnetic Properties of Rare Earth Metals* ed. R J Elliott (London: Plenum) pp 383–420
[11] Deutz A F, Brom H B, Huiskamp W J, de Jongh L J and Buschow K H J 1988 *Solid State Commun.* **68** 803–6
[12] Greidanus F J A M, de Jongh L J, Huiskamp W J, Furrer A and Buschow K H J 1983 *Physica* B **115** 137–55
[13] Deutz A F, Brom H B, Huiskamp W J, de Jongh L J and Buschow K H J 1989 *J. Magn. Magn. Mater.* **78** 31–9
[14] Deutz A F, Helmholdt R B, Moleman A C, de Mooij D B and Buschow K H J accepted for publication in *J. Less-Common Met.*
[15] Gignoux D and Givord F 1983 *J. Magn. Magn. Mater.* **31–34** 217–8
[16] Bleaney B 1963 *Proc. Roy. Soc.* A **276** 19–27
[17] Cooper B R 1972 In *Magnetic Properties of Rare Earth Metals* ed. R J Elliott (London: Plenum) pp 17–80
[18] Birgeneau R J 1973 In *AIP Conf. Proc. 10, part 2: Magnetism and Magnetic Materials* eds. C D Graham and J J Rhyne (New York: American Institute of Physics) pp 1664–88
[19] Hessel Anderson N, Jensen J, Smith H and Splittorff O 1980 *Phys. Rev.* B **21** 189–202